Supplemental Experimental Procedures

Experimental Model and Subject Details

All experiments were conducted with care and in accordance with the Columbia University institutional animal care guidelines. Both female and male mice were used for experiments, and were randomly assigned to experimental groups. Experiments were carried out on either C57BL/6 adult wildtype or transgenic Thy1-GCaMP6F animals at postnatal age of 1-3 months. No animals were used for previous or subsequent experimentation. Food and water was provided ad libitum. All mice were kept at a 12 hour light/dark cycle.

Method Details

Virus injections. 4-5 weeks prior to the actual experiment, wildtype animals were injected with AAV1-Syn-GCaMP6s (purchased from the University of Pennsylvania Vector Core). Mice were anesthetized with isoflurane (initial dose 2-3% partial pressure in air, then reduction to 1-1.5%). A small cranial aperture was established above left somatosensory cortex (coordinates from bregma: x 2,5mm, y -0,24mm, z -0,2mm) or visual cortex (coordinates from lambda: x = 2,5mm, z -0,2mm) using a dental drill. A glass capillary pulled to a sharp micropipette was stereotactically lowered into cortical layer 2/3. A 800nl solution of 1:1 diluted AAV1-Syn-GCaMP6s was slowly injected over 5 min at a depth of 200 µm from the pial surface using a microinjector (World Precision Instruments).

OGB-1 dye loading. Four experiments in this study included bulk loading of cortical neurons with Oregon Bapta Green-1 AM (OGB-1, Molecular Probes) 1 hour prior to imaging (Stosiek et al., 2003). OGB-1 was dissolved in 4µl of freshly prepared DMSO containing 20% Pluronic F-127 (Molecular Probes) and further diluted in 35µl of dye buffer [150mM NaCl, 2.5mM KCL, 10mM Hepes (pH 7.4)]. A glass capillary pulled to a sharp micropipette was slowly advanced at a 30° angle into the left somatosensory cortex using an ROE-200 manipulator (Sutter Instruments, Novato, CA) under visual control by two-photon imaging (20x water immersion objective, N.A.

0.5, Olympus) to a depth of 100-150µm depth beneath the pial surface. Then, the dye was slowly pressure-injected (10 psi, 8 min) using a picospritzer III system (Parker, Hollis, NH).

Experimental and surgical procedures. For imaging neural activity, wildtype animals were either injected with Oregon Bapta Green-1 AM (OGB-1, Molecular Probes) 1 hour prior to imaging or with AAV1-Syn-GCaMP6s into left somatosensory or visual cortex 4-5 weeks before the experiment. For the final set of experiments in awake mice, newly available transgenic Thy1-GCaMP6f (Dana et al., 2014) animals were used combining the fast kinetics of OGB-1 with the high signal to noise ratio of GCaMP6 calcium indicators (Chen et al., 2013). On the day of the experiment, mice were anesthetized with isoflurane (initial dose 2-3% partial pressure in air, then reduction to 1.0%). A small flap of skin above the skull was removed and a titanium head plate with a central foramen (7x7mm) was attached to the skull with dental cement above the left hemisphere (Fig 1 A). Then, a small craniotomy similar to previous descriptions (Miller et al., 2014) was carried out. Specifically, a circular section of the skull was thinned using a dental drill until a small piece (circa 2mm in diameter) of skull could be removed effortlessly with fine forceps. The dura mater was kept intact. For experiments during wakefulness, the craniotomy was covered with a thin glass cover slip (3x3mm, No.0, Warner Instruments) and fixed on the skull with dental cement. All mice involving survival procedures were allowed to recover for three days and habituated to the experimenter and the experimental setup. Directly prior to imaging, mice were briefly anesthetized with isoflurane again to establish a small cranial hole posterior to the glass cover as access site for the LFP pipette and the pipette containing 4-Aminopyridine or picrotoxin.

Microprism implant. For experiments involving multi-layer imaging, a small glass microprism (1x1x1 mm, Tower Optics) was implanted into the cortex similarly to previous descriptions (Andermann et al., 2013). To allow access for the LFP and 4-AP micropipettes during the experiment, a small part of the craniotomy remained uncovered in front of the prism face. Prior to insertion, microprisms were attached to a thin semi-round glass cover slip (broken in half 3x3mm

slip, blunt end aligned with prism edge) by use of a UV light sensitive glue (NOA 71, Norland Products) and a UV spot bulb (SB-100P Spot Bulb, Norland Products). For insertion, a small vertical incision was made through the dura mater into the cortex using a scalpel, in a region devoid of large blood vessels. Resulting bleeding was little, brief and the cut was gently rinsed with sterile saline. When no further bleeding could be observed, the prism - held by air suction - was positioned directly above the incision site using a stereotactic arm. Then the prism was slowly lowered 1 mm into the cortex. Once the coverslip edges hit the bone surrounding the craniotomy, its round edge was fixed on the skull first with silicon followed by dental cement on top of the silicon (higher stability). A small part of the craniotomy remained uncovered in front of the prism face and allowed access for the LFP and 4-AP micropipettes.

Animal training for experiments during wakefulness. After craniotomy and cover glass attachment, mice returned to their home cage and were allowed to recover for at least 3 days. Mice were given analgesics for pain relief (5mg/kg Carprofen i.p., quaque diem). All animals were habituated to the experimenter and the experimental setup, including short episodes of running freely on a rotating wheel while being head restrained under the microscope. Training was repeated until mice showed no signs of distress and comfortable movement or rest on the rotating wheel, usually after the second to third training session.

Two-photon calcium imaging. Activity of cortical neurons was recorded by imaging changes of fluorescence with a two-photon microscope (Bruker; Billerica, MA) and a Ti:Sapphire laser (Chameleon Ultra II; Coherent) at 940 nm through a 25x objective (water immersion, N.A. 1,05, Olympus). Resonant galvanometer scanning and image acquisition (frame rate 30.206 fps, 512 x 512pixels, 100-170µm beneath the pial surface) were controlled by Prairie View Imaging software. Multiple datasets were acquired consecutively over the course of an experiment (90000-150000 frames in total, with several momentary breaks interspersed for reasons of practicality). Since both OGB-1 and GCaMP6 imaging showed comparable calcium rise time dynamics (Chen et al.,

2013) during optical seizure break-in, similar cell recruitment time courses (Figure 1 and 2, S1 D) and no considerable differences in our spatiotemporal recruitment analysis, data was combined.

Electrophysiology and Ictal Model. For local field potential (LFP) recordings, a sharp glass micropipette (3-5 MΩ) filled with saline and containing a silver chloride wire was carefully advanced into the cortex (30° angle) under visual control to a depth of around 100 µm beneath the pial surface. The pipette tip was positioned close by the imaged area in anesthetized animals (Figure 1 A) or within the seizure initiation site during wakefulness (Figure 5 A). A reference electrode was positioned over the contralateral frontal cortex. LFP signals were amplified using a Multiclamp 700B amplifier (Axon Instruments, Sunnyvale, CA), low-pass filtered (300Hz), digitized at 1 kHz (Bruker) and recorded using Prairie View Voltage Recording Software alongside with calcium imaging. For induction of ictal events, another sharp glass micropipette containing 4-Aminopyridine (4-AP, 15 mM, 500 nl [total amount delivered = 7.5 nmol]) or picrotoxin (Ptx, 10 mM, 500 nl [total amount delivered = 5 nmol]) was slowly lowered (30° angle) into the cortex to a depth of ~480 µm. The pipette tip was positioned at a distance of around 1.5-3 mm caudally to the imaged area. Correct positioning of the pipette tip was ensured by a diagonal dry-run above the cortex preceding actual insertion. Chemoconvulsants were injected slowly by use of a Micro4 Micro-Syringe-Pump Controller (World Precision Instruments). In the case of secondary Ptx pressure perfusion in awake animals (Figure 6), Ptx was perfused (10 psi, 10 min) using a picospritzer III system (Parker, Hollis, NH). Electrographic seizure onset time points were determined mathematically by mean and standard deviation of LFP recordings. The first time point exceeding > 5 std from the interictal LFP rectified voltage was defined as seizure onset and confirmed by visual inspection.

Image Analysis. Raw movie files were processed to correct translational brain motion using the in house written MOCO motion correction algorithm as a plugin in ImageJ (Dubbs et al., 2016). Then, cell regions of interest (ROIs) were identified in a semi-automated fashion by using custom

written software in MATLAB (Caltracer 3 beta, available on our laboratory website: http://www.columbia.edu/cu/biology/faculty/yuste/methods.html) followed by manual confirmation. Because of pronounced and synchronous fluorescence changes of surround neuropil during ictal conditions, halo subtraction procedures could lead to distortions of calcium transients of individual cells. Therefore, we applied ROI shrinkage (ROI soma outline minus 1.5 pixels radially), which has been successfully used to minimize bleed-in of surround neuropil fluorescence (Hofer et al., 2011). Cells with low signal to noise ratio or no apparent calcium transients were excluded from further analysis. Individual cells that were lost over the course of the experiment due to axial movement of the imaged focal plane during local 4-AP injection were also excluded from analysis. Individual cell fluorescence was calculated as the average across all pixels within the ROI. The same approach was taken for experiments involving tiling of the field of view into 36, 12, 4 or 2 tiles instead of defining individual cell ROIs (Fig. S2 A). The ΔF/F of individual ROI traces was calculated by subtracting the mean of the lowest 25% of values within a 1000-frame sliding window from each value at the center of this window, divided by the mean of the lowest 25% of the window. Finally, individual traces were filtered with a 2-second lowess smoothing envelope that is tolerant of sharp changes of fluorescence. This step minimized tissue pulsation artifacts in the extracted traces, which become more apparent during high speed resonant scanning as compared to optical recording involving conventional galvanometers.

Cell Analyses. In order to identify the recruitment time-point of individual cells to ictal activity, we used the first discrete derivative (slope) of the ΔF/F traces assuming that the sharpest change in fluorescence correlates best with maximal recruitment to ictal activity.

Recruitment reliability. To detect cells with a reliable recruitment pattern across multiple ictal events, we took two different approaches. The first approach involved the division of each optical seizure break-in of an experiment into three equal time bins (early, intermediate and late, or 1, 2 and 3, Fig. S2 C, top panel), yielding a single “bin” per cell per seizure event. Similarly to a z-

score, we also calculated a relative recruitment score (rr-score) for every single cell as follows. With respect to the median frame within each ictal onset period (Y50, the frame wherein the cumulative number of recruited cells first equaled or exceeded 50% of all analyzed cells), each cell was assigned an onset frame lag (Xn = individual cell onset frame. Frame lag = Xn – Y50). Each cell's lag was then divided by the standard deviation of all lags across all cells within a seizure event (*∂*). Specifically, rr-scores were calculated as

$Z = (Xn - Y50) / \partial$

This enabled a flexible quantification of the temporal recruitment ordering of a cell relative to a given network-wide event, and was therefore independent of ictal duration and symmetry (Fig. S2 C, bottom panel). From the resulting "observed recruitment matrices" (e.g. 100x10 matrix in the case of 100 cells and 10 ictal events) of either time bin categories (1, 2, or 3) or rr-scores, the standard deviation (std) was obtained for every individual cell across all events (resulting in a 100x1 vector). Then, the observed recruitment matrix was used to create a shuffled surrogate where each individual cell's identity was randomly re-assigned to an observed recruitment time-point during an individual ictal event thereby maintaining each seizure's cell recruitment time-point distribution (Fig. S2 D) but randomizing relative recruitment ordering across cells. This action was repeated 1000 times (shuffling the dataset >1000 times resulted in a change only affecting the 3rd decimal point) calculating a pool of 100000+ std values. Cells with an observed std < 95% of all surrogate values were defined as "reliable". Finally, a reliability index was calculated as the percentage of reliable cells/tiles out of all analyzed cells/tiles (e.g., if 10 out of 100 cells are reliable, the reliability index will be 10%).

Spatiotemporal Clustering. In order to test for the presence of spatially patterned progression of ictal events, we first ordered cell recruitment points in time (from early to late recruitment) during each individual ictal event of an experiment and divided each dataset into recruitment time quartiles (1-25%, 26-50%, 51-75%, 76-100%). For each seizure, the mean distance of cell

coordinates (x,y within imaged area) of individual quartiles were calculated to either i) the mean coordinate of the respective quartile, or ii) the mean coordinate of all recorded cells. Then, these distances were compared to each other with a bivariate ANOVA (see below) to test the hypothesis that individual cell onset times can be predicted from their relative location in space (Fig. S2 E).

Assessment of layer-specific temporal delays. We grouped small local cell populations together in spatial tiles of 100 µm width to assess lateral delays of adjacent tiles and vertical delays of tiles situated above each other (Fig. 4 A). First, the recruitment of each of the tiled cell populations for every individual seizure was derived, as with single cell recruitment, by calculating the first discrete derivative (slope) of the population ΔF/F trace for each constituent cell and averaging over cells within tiles. Temporal delays (frame lags) between tiles were quantified as the difference in recruitment frames between neighboring tiles (tile [prox] - tile[dist] or tile[LII/III] - tile[LV]). Negative frame lags would indicate that the tile proximal to the 4-AP injection site was recruited before the more distal adjacent tile (lateral delays), or that the LII/III tile was recruited prior to the corresponding LV tile (vertical delays; Fig. S3 D).

Quantification and Statistical Analysis

All data were analyzed using custom written code in MATLAB (MathWorks, Inc). Error bars on bar plots and shaded areas in graph plots indicate s.e.m.. Reliability indices of cells, 36 tiles, 12 tiles and 4 tiles were compared using one-way ANOVA (3 degrees of freedom [df]). For statistical analysis of spatio-temporal clustering, we used bivariate ANOVA analysis of mean distance differences (df = 3). Spatial tile onset order distributions (i.e. number of recruitments occurring first in proximal vs distal and superficial vs deep; Fig. 4 B and C) were compared to an even distribution (16 proximal / 16 distal, 16 superficial / 16 deep) with a 2X2 chi-square test (df = 1). With respect to optical seizure invasion rate, cellular recruitment durations, duration stdev, LFP to Calcium delays, and delay stdev, 2 experimental groups (Ptx-1 versus Ptx-2, Fig. 6 I, K, L) were compared across experiments using Mann Whitney test.

Additional Resources

Both MOCO (motion correction) and Caltracer (extraction of calcium signals) are available on the Yuste lab website: http://www.columbia.edu/cu/biology/faculty/yuste/methods.html

Resource Table

Experimental Models: Mouse lines		
C57BL/6 wildtype	Jackson Laboratory	RRID:IMSR_JAX:000664
C57BL/6J-Tg(Thy1-GCaMP6f)GP5.11Dkim/J	Jackson Laboratory	RRID:IMSR_JAX:024276
Chemicals (Pharmacological compounds)		
Oregon Bapta Green-1 AM	Invitrogen	Cat # O6807
4-Aminopyridine	Sigma-Aldrich	Cat # 275875; CAS:504-24-5
Picrotoxin	Sigma-Aldrich	Cat # P1675; CAS: 124-87-8
Recombinant DNA		
AAV1-Syn-GCaMP6s-WPRE-SV40	U Penn Vector Core	Cat # AV-1-PV2824
Software and Algorithms		
ImageJ	https://imagej.nih.gov/ij/	
Moco	http://www.columbia.edu/cu/biology/faculty/yuste/methods.html	
MATLAB(R2014b)	MathWorks	
Caltracer3beta	http://www.columbia.edu/cu/biology/faculty/yuste/methods.html	
Adobe Illustrator CS6	Adobe	

Supplemental Figures

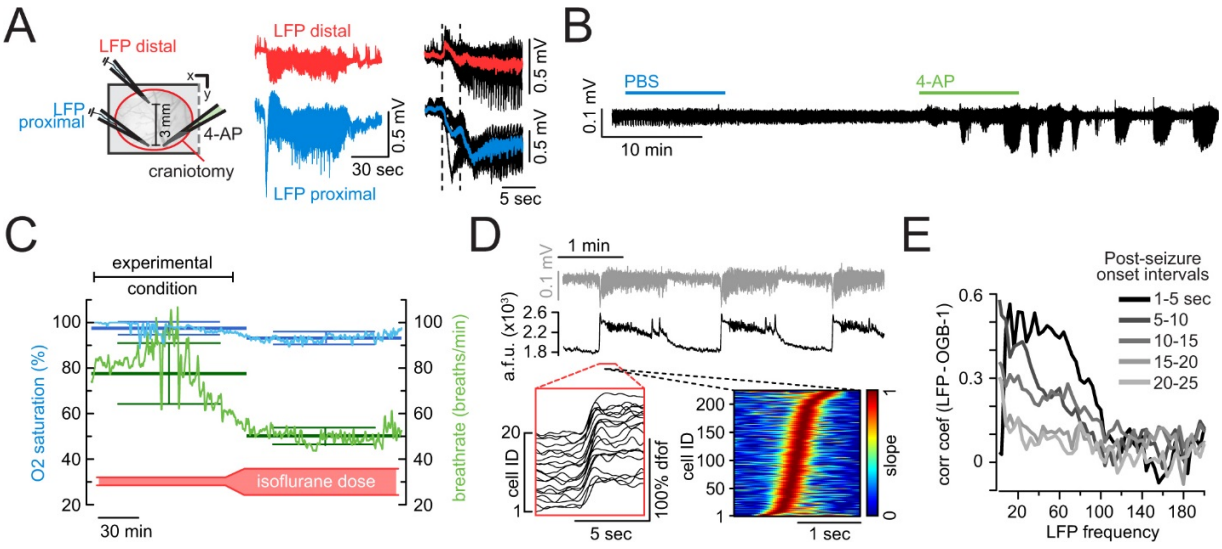

Figure S1, Related to Figure 1. (A) Distance dependent reduction in LFP signal amplitude during electrographic seizures, while timing of the LFP signal is preserved. Left: Schematic depiction of experimental setup; two LFP pipettes (blue = proximal, red = distal) being spaced 3 mm apart. A third pipette containing 4-AP (green, 15 mM, 500 nl [total amount delivered = 7.5 nmol]) was inserted at the site of the proximal LFP pipette, and advanced to a depth of ~480 µm. The reference electrode was located at contralateral frontal cortex. Middle: Individual electrographic seizure recorded at the two LFP sites. Note how the timing of the electrographic seizure is preserved in both sites, yet with a reduced amplitude at the distant electrode. Right: Superposition of 5 consecutive electrographic seizures recorded at the two LFP sites (top = distal, bottom = proximal). **(B)** Epileptiform activity occurs only upon local injection of a chemoconvulsant. First, 500 nl sterile PBS were injected at the seizure initiation site, upon which no epileptiform activity could be detected for a protracted period of time. Only following the injection of the chemoconvulsant (4-AP, 500 nl, 15mM, total dose administered = 7.5 nmol), did epileptiform activity and a series of full blown ictal events develop. **(C)** Peripheral blood oxygenation remains stable for hours during isoflurane anesthesia. Representative example of vital parameters during shallow anesthesia (the experimental condition in this study) and deeper anesthesia over the course of 4 hours under ventilation with isoflurane (vaporized in room air). Vital parameters were measured via a paw sensor, which optimally reads out peripheral tissue oxygenation. During shallow anesthesia, the isoflurane dose (red bar at the bottom indicates low or increased dose) was kept at ~1% partial pressure in air, while during deeper anesthesia the isoflurane dose was

~1.5% partial pressure in air. During shallow anesthesia, the mean breath rate was 77.6242/min (std = 13.0260) and peripheral oxygen saturation remained continually near 100% (mean = 97.4945, std = 2.8668). After two hours (experiments usually did not continue beyond this time period), isoflurane concentration was increased and vital parameters were further monitored. The mouse was kept under this condition for another two hours. With the increased isoflurane dose, the breath rate lowered to a mean of 50.1682/min (std = 3.4451), while peripheral blood 02 saturation remained high (mean = 93.2454, std = 2.7998). This underscores that peripheral tissue oxygenation remains sufficiently high for hours of isoflurane anesthesia vaporized in room air, much beyond the usual time period of a typical experiment in this manuscript, and even with increased doses of isoflurane (that were not employed in this study). **(D)** Representative exp.: LFP (gray trace) recording and corresponding population average calcium transient (black trace, OGB-1, imaging depth ~150µm beneath the pial surface) after 4-AP injection (see also movie S1). Red box: calcium transients of 20 representative cells after injection of 4-AP during ictal break-in. Black box: Cell recruitment to ictal activity ordered in time by maximum slope of calcium transients. **(E)** Representative exp. under anesthesia (OGB-1, 224 cells, 9 seizures). Correlation (r) between population mean fluorescence and instantaneous LFP power (250ms windows, hanning tapered). Different gray tones correspond to consecutive 5 second intervals of the electrographic seizures. During electrographic seizure onset, the imaged rise in calcium was well correlated with the typical increase in spectral power of the ictal LFP signal over a wide frequency range (1-100Hz). With the transition of the electrographic seizure from the tonic to the clonic phase, strength in correlation between the LFP gamma range and the calcium signal decreased.

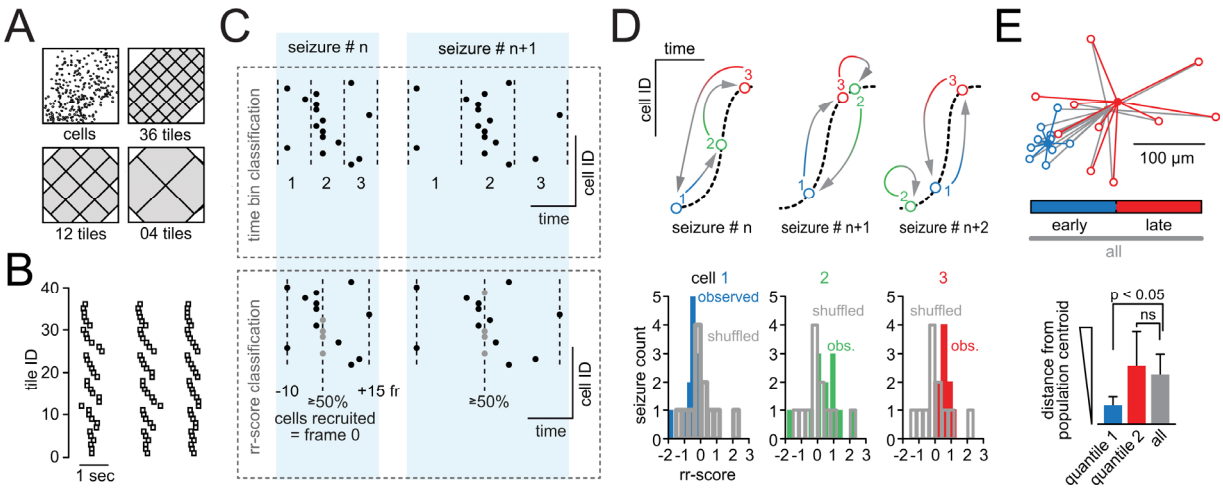

Figure S2, Related to Figure 2. (A) ROI (region of interest) registration scheme. **(B)** The same three consecutive optical seizure break-ins shown in Fig. 2 B are plotted directly next to each other in their raw temporal order (36 tile ROIs), showing conserved temporal regularity of ictal propagation. Each rectangle represents the recruitment time point of an individual tile. **(C)** Two analytical approaches as a means to quantify temporal reliability at the single cell scale. Schematic analysis of two consecutive seizures (shaded in light blue). Upper panel: Time bin classification: Division of individual ictal break-in periods into three equally sized time bins (dotted lines), regardless of the onset duration (early, intermediate and late = 1, 2 and 3). Lower panel: rr-score classification for every individual cell with respect to the median recruitment frame (50% frame = dotted line in the middle, cells recruited at this frame in gray). Cells recruited before this frame will have negative frame lags, cells recruited after this frame will have positive frame lags. In this approach, relative temporal network recruitment structure is maintained, even during asymmetrical stretching of absolute temporal network recruitment. **(D)** Schematic depiction of reshuffling approach to detect cells showing above chance level recruitment reliability. Upper panel: Sketch of 3 cells (blue, green, red) across three seizure break-ins (dotted lines). During each seizure, each cell has an observed recruitment time point and a shuffled one. Note that for the reshuffling procedure in each seizure, the cell identities are randomly redistributed along the maintained temporal population recruitment distribution. Lower panel: three representative cells from a real experiment, with their observed rr-score distributions for 12 seizures (= 12 rr-scores for each cell; colored bars), and their respective shuffled rr-score distributions (gray outlined bars; 1000 shuffle repetitions, displayed bars are averaged for visualization). Note that cell 1 has observed recruitment time points consistently prior to the 50% recruitment frame, cell 3 gets recruited consistently later than the 50% onset frame, and cell 2 shows a varied recruitment

pattern. Importantly, the shuffled distributions are near identical across all cells. Consequently, cell 1 and 3 would show smaller rr-score std than 95% of the (thousands of) randomized "cells", therefore they would be defined as "reliable". On the other hand, cell 2 does not show reliable recruitment (largely overlapping value distribution with shuffled equivalent). **(E)** Schematic depiction of the bivariate cluster analysis applied in this study. Top: For ease of visualization, only two quantiles (blue = 50% earliest recruited cells, red = 50% latest recruited cells) are displayed (analysis of experiments contained quartiles), for a single seizure. Each quantile contains 10 cells. Each outlined circle corresponds to the spatial coordinate of an individual cell, each filled circle to the respective quantile centroid (blue = 1st quantile, red = 2nd quantile, gray = all; centroid = mean spatial coordinate). Note: quantiles were first derived based only on temporal onset, irrespective of space. For each quantile, the mean distance of cell coordinates to the quantile centroid was compared to the mean distance of all analyzed cells to the overall centroid (gray). Bottom: Arbitrary mean distance + std for each quantile for the single seizure shown on the left (actual analysis contained all seizures of an individual experiment). Cells belonging to the early 50%ile (blue) cluster spatially, cells belonging to the late 50%ile (red) do not.

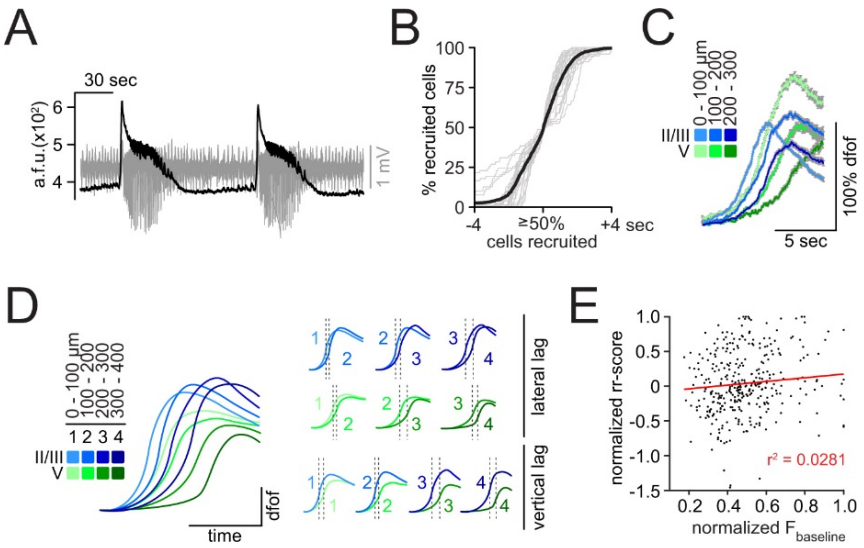

Figure S3, Related to Figures 4 and 5. (A) Average calcium transient of imaged FOV (black trace, GCaMP6s) and corresponding LFP (gray trace) after 4-AP injection. **(B)** Superposition of all analyzed multilayer seizure break-ins (gray) centered around the 50 % recruitment frame; black graph represents mean temporal recruitment (n = 4 experiments, total # of seizures = 32 [8 ± 3.6 s.e.m.], total # of cells analyzed = 334 [84 ± 13 s.e.m.], cell number in % for comparability across experiments). **(C)** Additional experiment paradigmatically illustrating horizontal and vertical population recruitment time lags during seizure invasion. Population average calcium transients within layer-specific spatial tiles (100 µm width), gray shades represent s.e.m. (# of seizures = 3, # of cells analyzed = 74, # of tiles = 6). **(D)** Schematic depiction of analysis of layer-specific lateral and vertical recruitment time lags. Small local cell populations were grouped together in spatial tiles of 100 µm width within the field of view (4 tiles [LII/III], 4 tiles [LV]). Population average calcium transients of individual tiles are shown for a paradigmatic seizure. To calculate the lateral time lag of a given pair of adjacent tiles, the recruitment frame of the tile distal from the 4-AP injection site is subtracted from the recruitment frame of the tile proximal to the injection site (tile2 – tile1, tile3 – tile2, tile4 – tile3) and the average lag is derived. To calculate vertical time lags between corresponding tiles in LII/III and LV, the same scheme is used (tile1[LII/III] – tile1[LV], tile2[LII/III] – tile2[LV] and so forth). **(E)** Correlogram of cellular baseline fluorescence (Transgenic GCaMP6f) versus rr-scores. Values are max-normalized for comparability across animals. The relationship between cellular baseline fluorescence and temporal recruitment is negligible. 5 exp., 360 cells, 26 seizures. R = 0.1675, R2 = 0.0281. The effect accounts for 2.8% of the variance in the data.

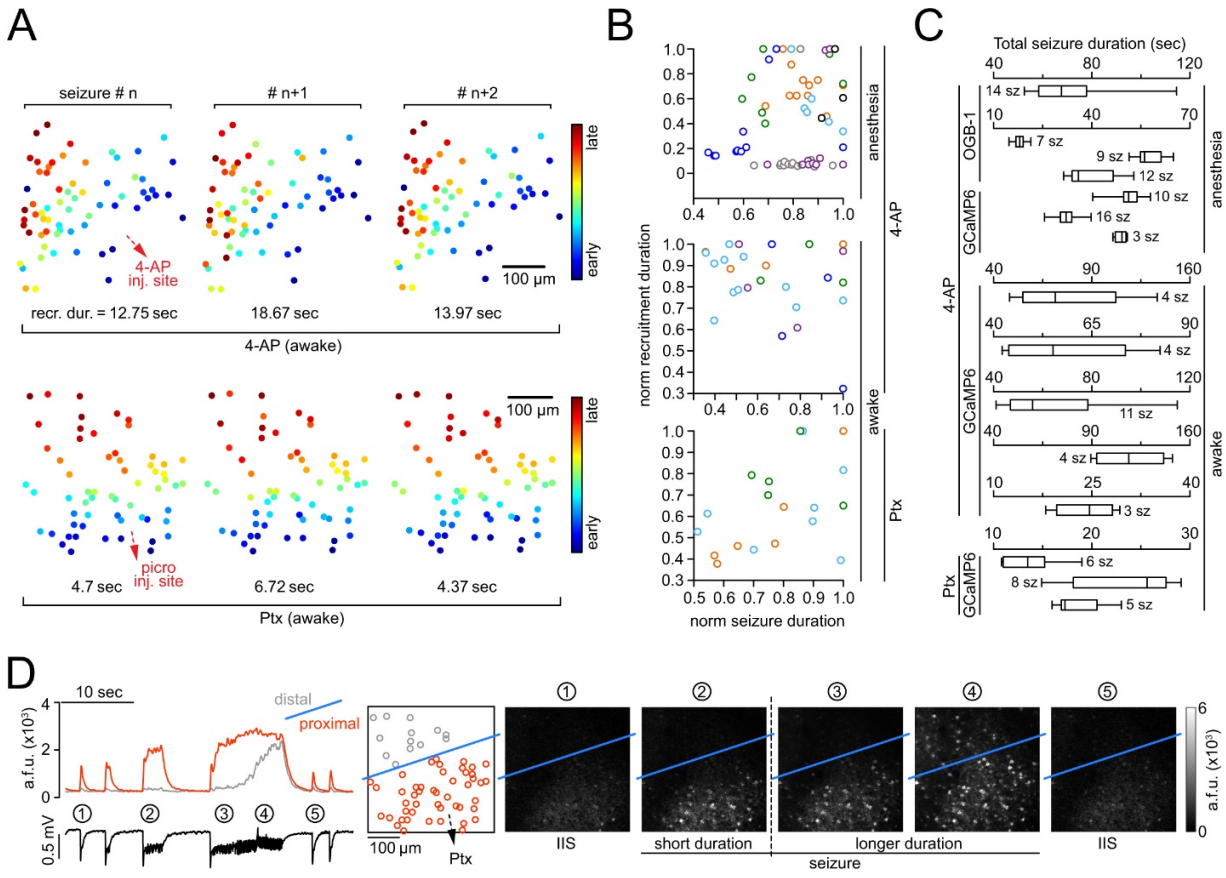

Figure S4, Related to Figure 6. (A) Spatiotemporal contour plots of cell recruitment in three consecutive seizures after either 4-AP (top) or Ptx (bottom) injection. Each dot represents an individual cell. 4-AP or Ptx injection site (red arrow) is located in layer V, ~2mm (4-AP) or ~1.5mm (Ptx) posterior to the imaged FOV in somatosensory cortex. Note how relative cellular recruitment is grossly preserved across seizures in both experimental models, while absolute recruitment durations vary greatly on the scale of seconds. **(B)** There is no systematic relationship between total seizure duration (x axis) and local population recruitment duration (y axis). x and y axes are normalized for comparability across animals. Each circle represents an individual seizure, colors represent individual experiments. Top: Local 4-AP injection under anesthesia; n=7 exp.; for 6 exp. no significant correlation (p = 0.612, 0.437, 0.272, 0.279, 0.21, 0.728), 1 exp. significant negative correlation (light blue, 6 seizures, p = 0.043, R = -0.826). Middle: Local 4-AP injection during wakefulness; n=5 exp.; no significant correlation (p = 0.478, 0.163, 0.962, 0.421, 0.957). Bottom: Local Ptx injection during wakefulness; n=3 exp.; for 2 exp. no significant correlation (p = 0.564, 0.804), 1 exp. significant positive correlation (orange, 6 seizures, p = 0.006, R = 0.938). **(C)** Total electrographic seizure durations vary within and across exp.. Box plots of 15 exp. in the

propagation area (7 anesthesia, 8 wakefulness): Boxes represent 25%ile to 75%ile of absolute seizure duration, bands inside boxes display median seizure duration. **(D)** Representative example highlighting that only after a second Ptx injection (pressure controlled, picospritzer, 10 psi. 10 min), but not after the first Ptx injection (as performed for all 4-AP exp. and 4 Ptx exp.), Ptx diffuses into the imaged territory (initiation site located 1.5-2 mm posterior to the imaged area). Shown here is the condition where Ptx diffusion across the field of view is incomplete, resulting in differential calcium dynamics (left, top [gray or orange]) of groups of cells within the field of view (contour plot, distal [gray] and proximal [orange] sub-populations, demarcation line [blue]) with respect to the LFP signals (left, bottom [black], recorded at the initiation site). Five specific events are additionally displayed on the right as average calcium images of the field of view (Event 1 and 5 = interictal spikes in LFP [IIS], 2 = short duration ictal event, 3 and 4 = longer duration ictal event). Note how the proximal cell population calcium shows a reliable response to every LFP event, while the distal population (gray) is only slowly optically invaded, and in a delayed fashion (event 4), during sustained ictal activity in the LFP.

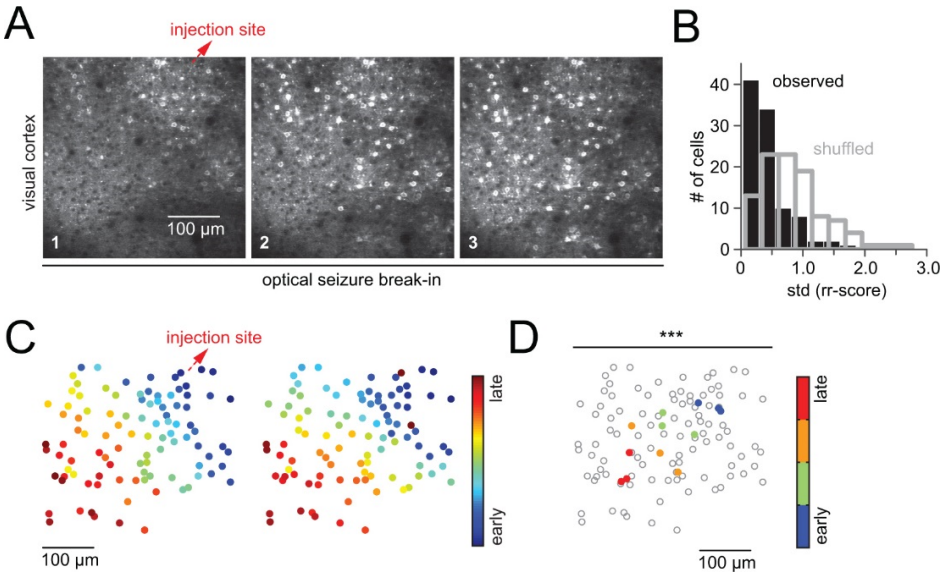

Figure S5. Consistent features of microscale seizure progression can be found across sensory cortices.

(A) Three representative average images of the optical break-in during microscale seizure progression into visual cortex (injection site located at a distance of ~2 mm anterior to the FOV). **(B)** Representative example. Observed (black) versus shuffled (blue) rr-score std distribution (100 cells, reshuffling procedure performed 1000 times), indicating that the variability of relative temporal onset order was less than would be expected by chance at the individual cell level (cell reliability index (rr-score, 2 exp.) = 0.3342 ± 0.084). **(C)** Spatiotemporal maps of cell recruitment of the same experiment shown in A and B in two consecutive seizures indicating grossly preserved relative recruitment. Each dot represents an individual cell. 4-AP injection site (red arrow) is located ~2 mm antero-medially from the imaged FOV. **(D)** Same experiment, spatial averages of temporally defined population quartiles (25% earliest recruited cells, 25-50%, 50-75%, 75-100%) across 3 consecutive seizures show consistent spatiotemporal propagation (bivariate ANOVA p = 0.000429, F[3,8] = 15.886; 2nd exp.: 3 seizures, p = 0.0000327, F[3,8] = 41.224). Each colored dot represents the average coordinate of all cells belonging to the respective quartile. Gray circles represent individual cells.

Supplemental References

Andermann, M.L., Gilfoy, N.B., Goldey, G.J., Sachdev, R.N., Wolfel, M., McCormick, D.A., Reid, R.C., and Levene, M.J. (2013). Chronic cellular imaging of entire cortical columns in awake mice using microprisms. Neuron *80*, 900-913.

Chen, T.W., Wardill, T.J., Sun, Y., Pulver, S.R., Renninger, S.L., Baohan, A., Schreiter, E.R., Kerr, R.A., Orger, M.B., Jayaraman, V.*, et al.* (2013). Ultrasensitive fluorescent proteins for imaging neuronal activity. Nature *499*, 295-300.

Dana, H., Chen, T.W., Hu, A., Shields, B.C., Guo, C., Looger, L.L., Kim, D.S., and Svoboda, K. (2014). Thy1-GCaMP6 transgenic mice for neuronal population imaging in vivo. PLoS One *9*, e108697.

Dubbs, A., Guevara, J., and Yuste, R. (2016). moco: Fast Motion Correction for Calcium Imaging. Front Neuroinform *10*, 6.

Hofer, S.B., Ko, H., Pichler, B., Vogelstein, J., Ros, H., Zeng, H., Lein, E., Lesica, N.A., and Mrsic-Flogel, T.D. (2011). Differential connectivity and response dynamics of excitatory and inhibitory neurons in visual cortex. Nature neuroscience *14*, 1045-1052.

Miller, J.E., Ayzenshtat, I., Carrillo-Reid, L., and Yuste, R. (2014). Visual stimuli recruit intrinsically generated cortical ensembles. PNAS *111*, E4053-4061.